cardiovascular magnetic resonance imaging (CMR) in patients with heart failure

Foroughi Asl R,MD
Consultant Cardiologist
Cardiac Imaging

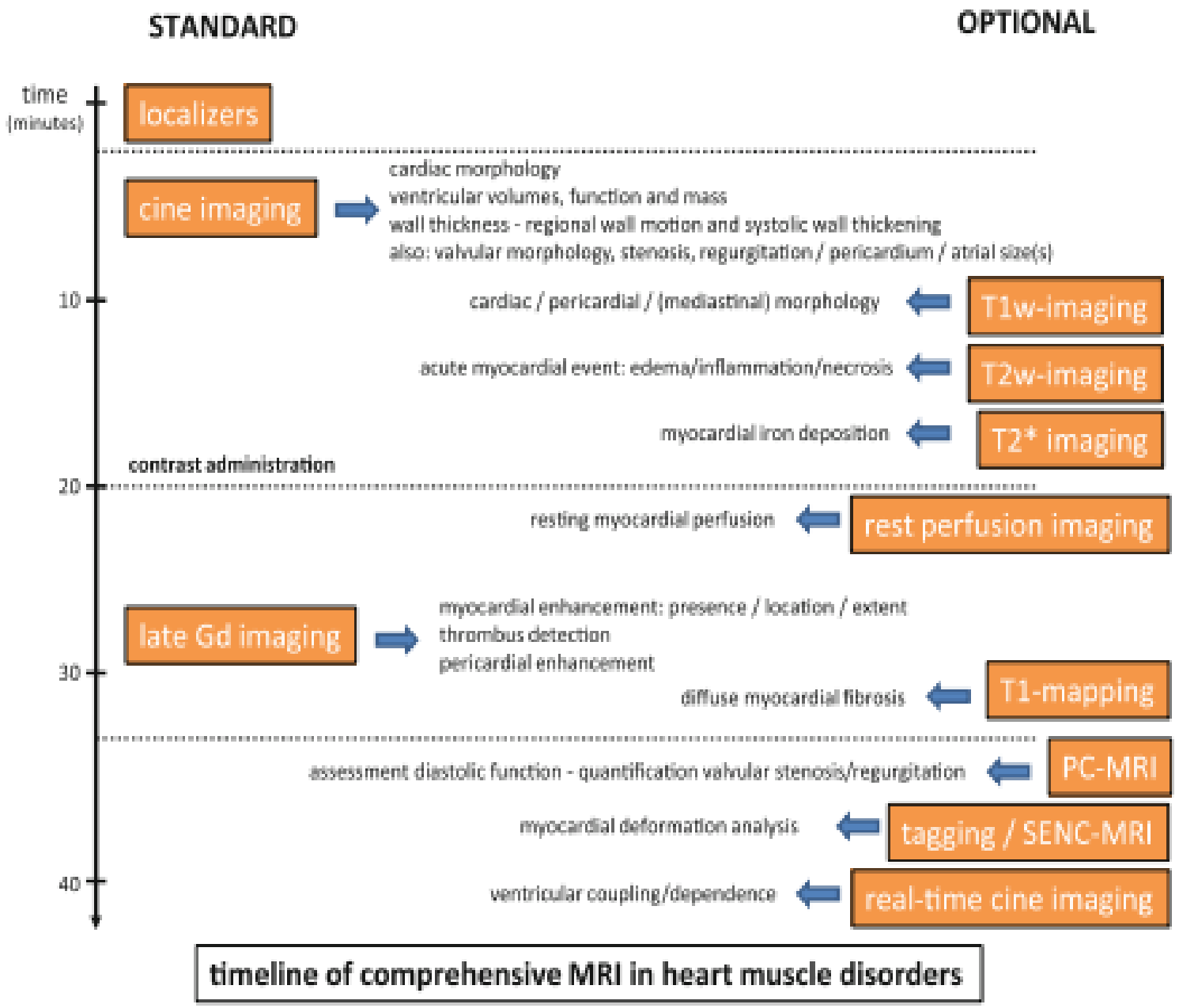

timeline of comprehensive MRI in heart muscle disorders

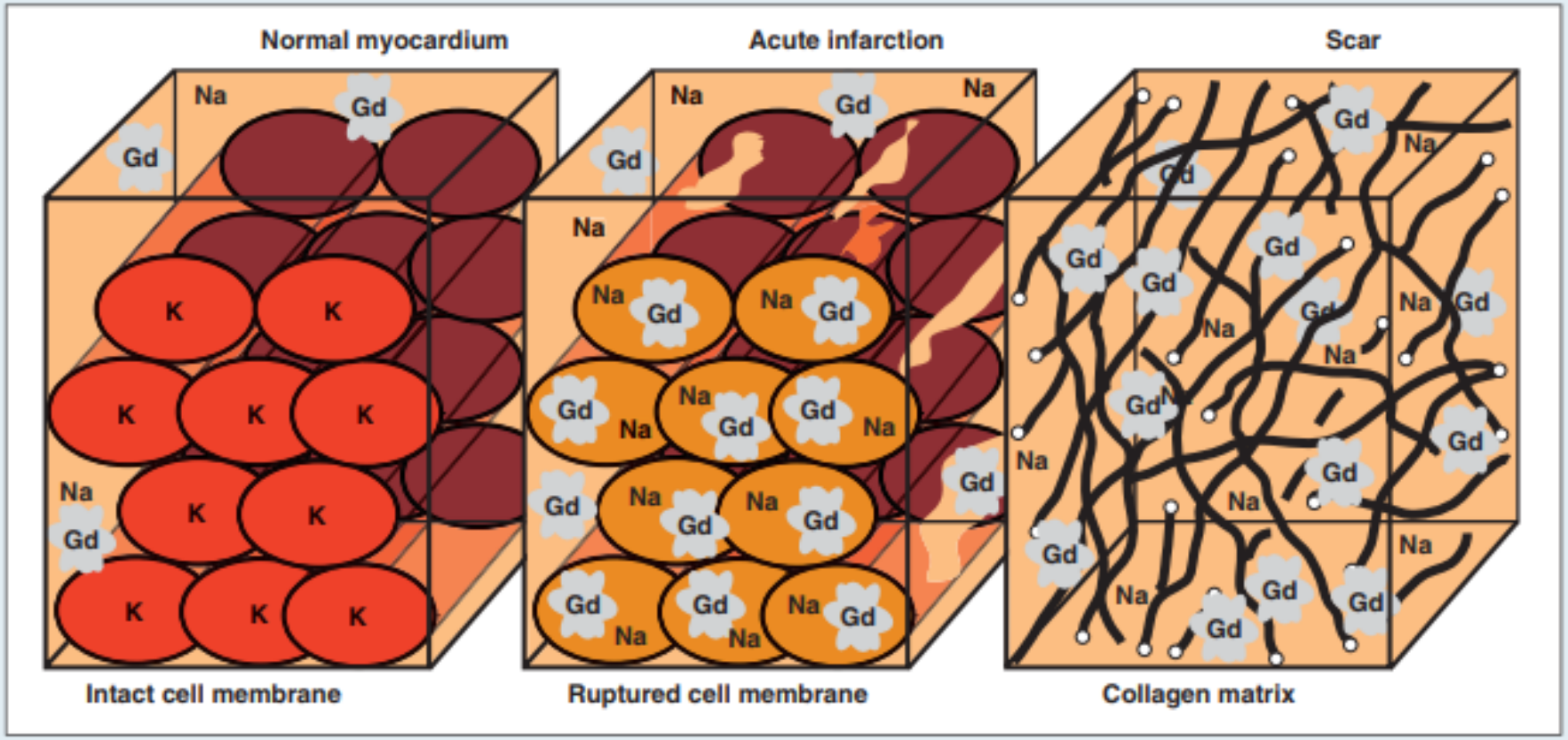

Figure 19-7 The physiologic basis of hyperenhancement in DE-CMR. In normal myocardium, two points should be noted. First, myocytes are densely packed, and total tissue volume is predominantly intracellular (≈ 80% of the water space). Second, gadolinium contrast media does not cross cellular membranes, and thus is limited to the extracellular (intravascular and interstitial) space. The result is that the volume of distribution of gadolinium contrast in normal myocardium is quite small (≈ 20% of water space), and one can consider viable myocytes as actively excluding contrast media. In acutely infarcted regions the myocyte membranes are ruptured, allowing gadolinium to passively diffuse into the intracellular space. The result is an increased concentration of gadolinium at the tissue level and therefore hyperenhancement occurs. Myocardial scar is characterized by a dense collagenous matrix; however, at a cellular level the interstitial space between collagen fibers may be significantly greater than the interstitial space between the living myocytes that is characteristic of normal myocardium. Thus the concentration of gadolinium in scar is greater than in normal myocardium because of the expanded volume of distribution and the regions of scar appear hyperenhanced by DE-CMR.

gold standard noninvasive test for determining the underlying causes, prognostic value, guiding therapy

acute tissue injury: edema and necrosis

in nonischemic heart failure: fibrosis, infiltration, and iron overload

LGE

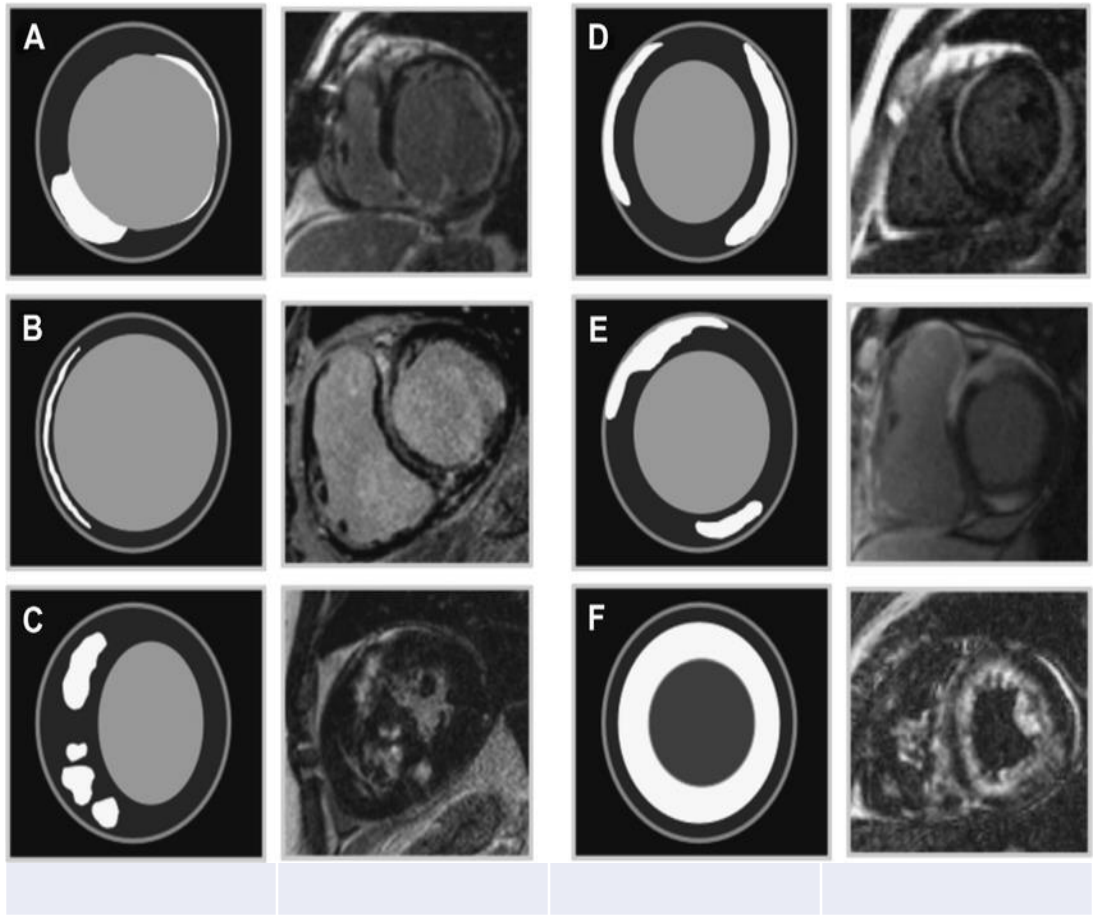

- LGE patterns identied by late gadolinium enhancement imaging in patients with ischemic and nonischemic cardiomyopathy. (A) Ischemic cardiomyopathy: patient with transmural inferoseptal and nontransmural lateral wall representing infarctions of the right coronary artery and circumex territories. (B) Dilated cardiomyopathy: patient with midwall "striae" throughout the interventricular septum. (C) Hypertrophic cardiomyopathy: patchy midwall within the hypertrophied septal wall segments. (D) Viral myocarditis: epicardial-based in the anteroseptal and inferolateral walls. (E) Sarcoidosis: dense epicardial-based of the anteroseptal and inferior walls. This case also shows right ventricular involvement. (F) Amyloidosis: diffusedglobal, subendocardial to epicardial involving both the left and the right ventricle.

AMYL2/PRE/POST CONTRAST

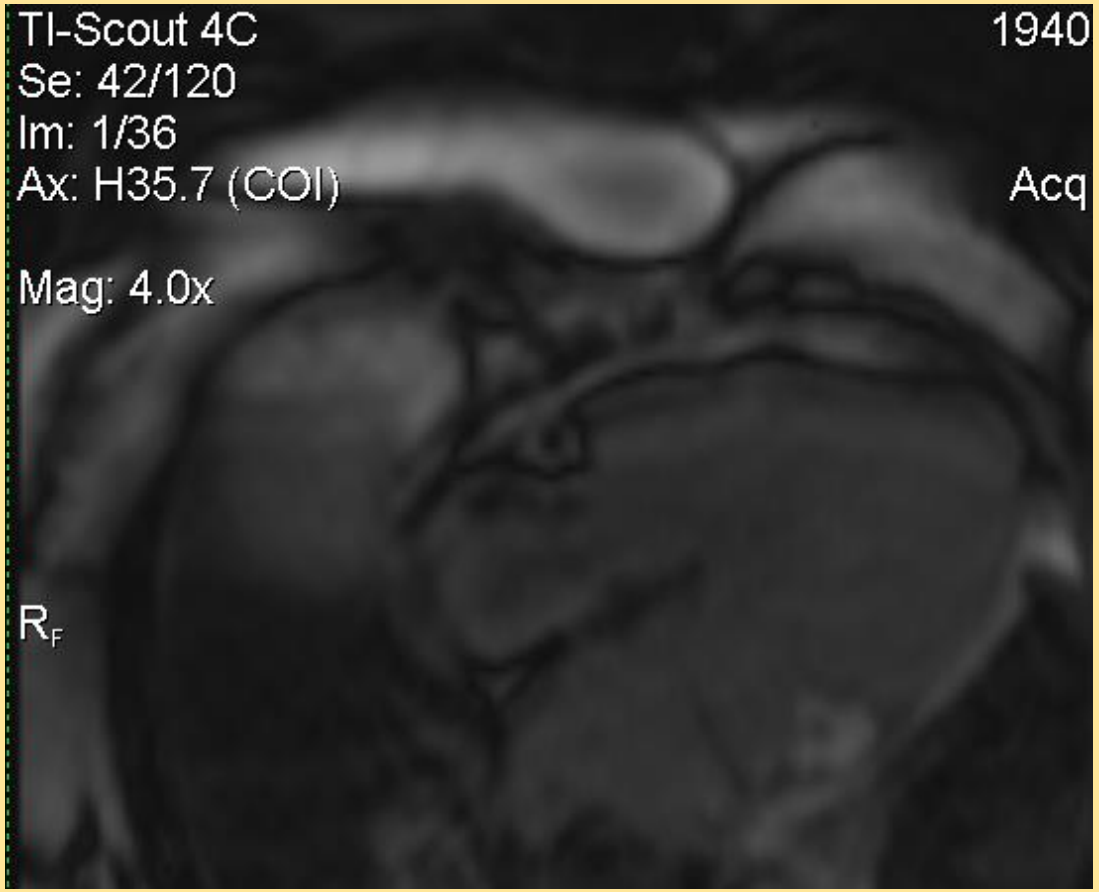

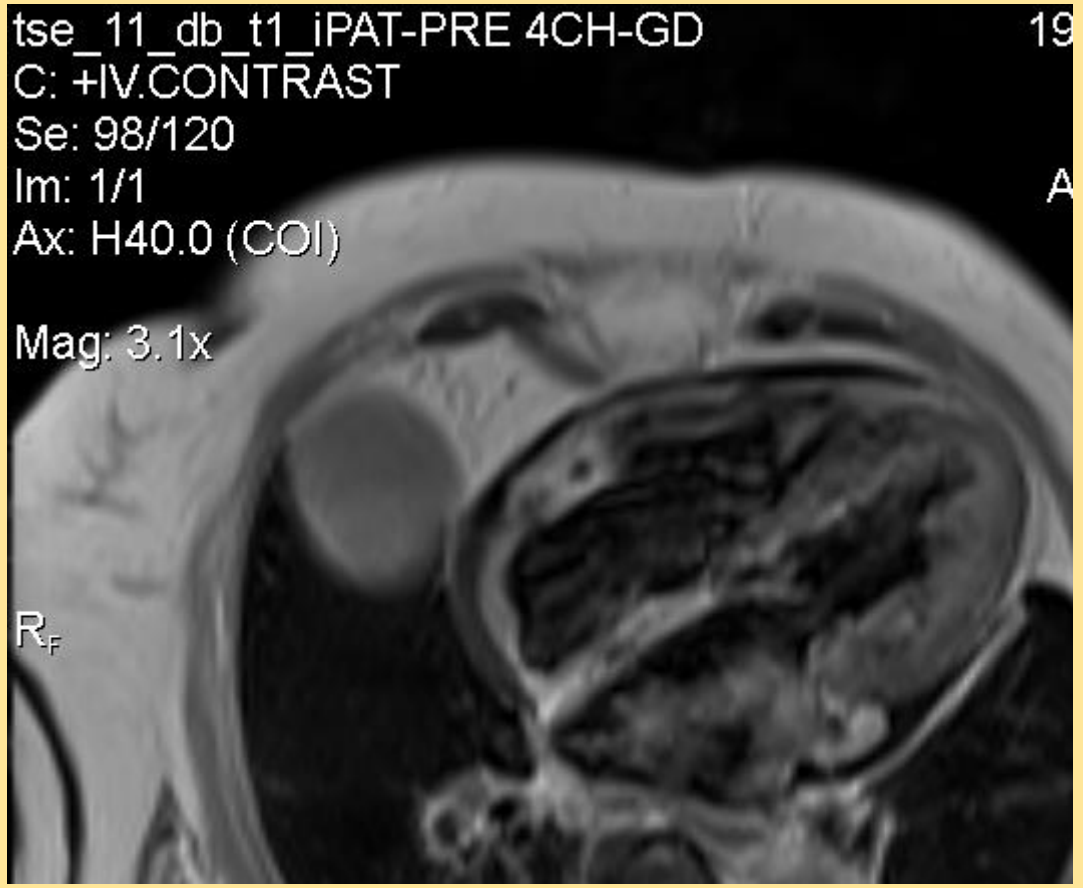

SHEPHERD’s CROOK PATTERN(sign)

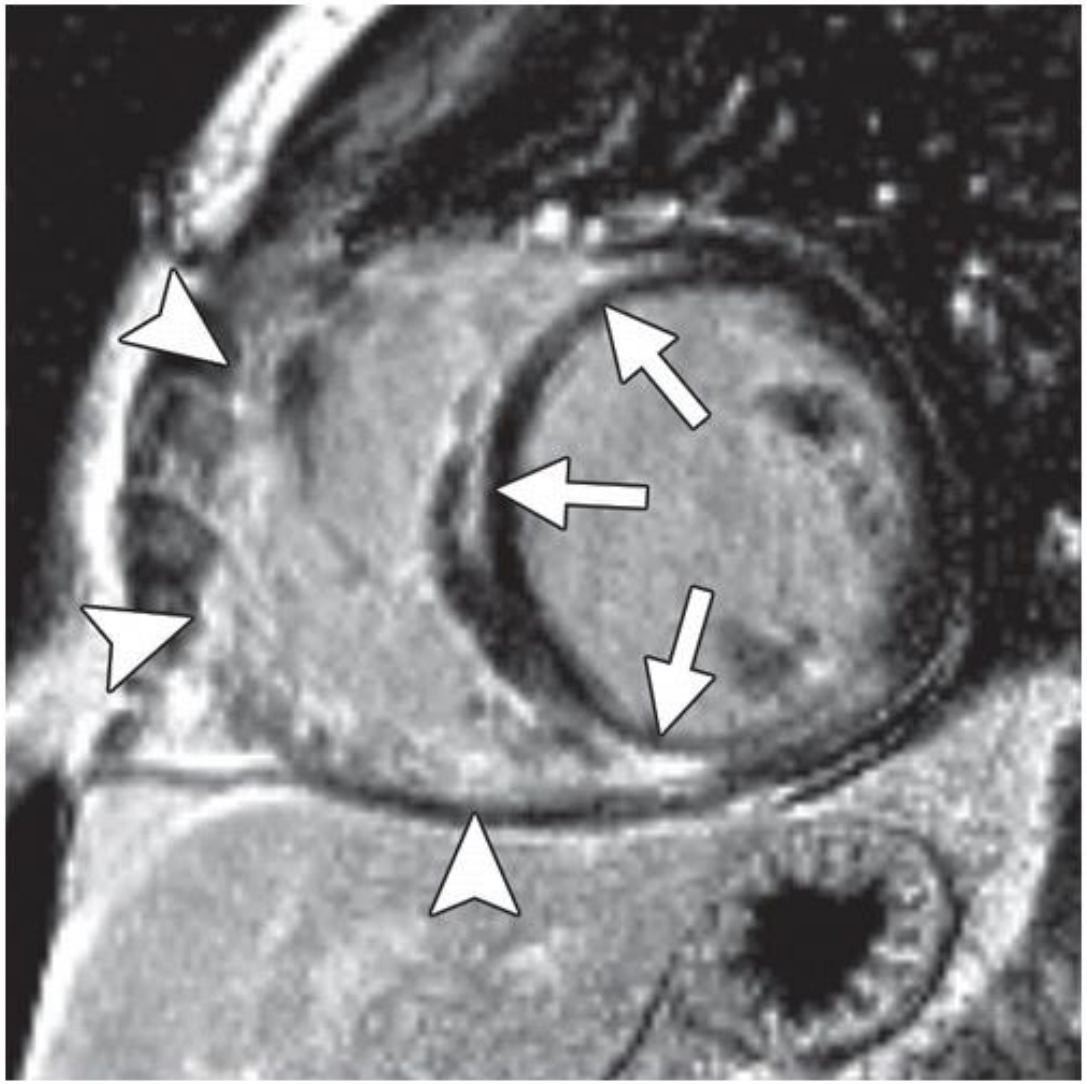

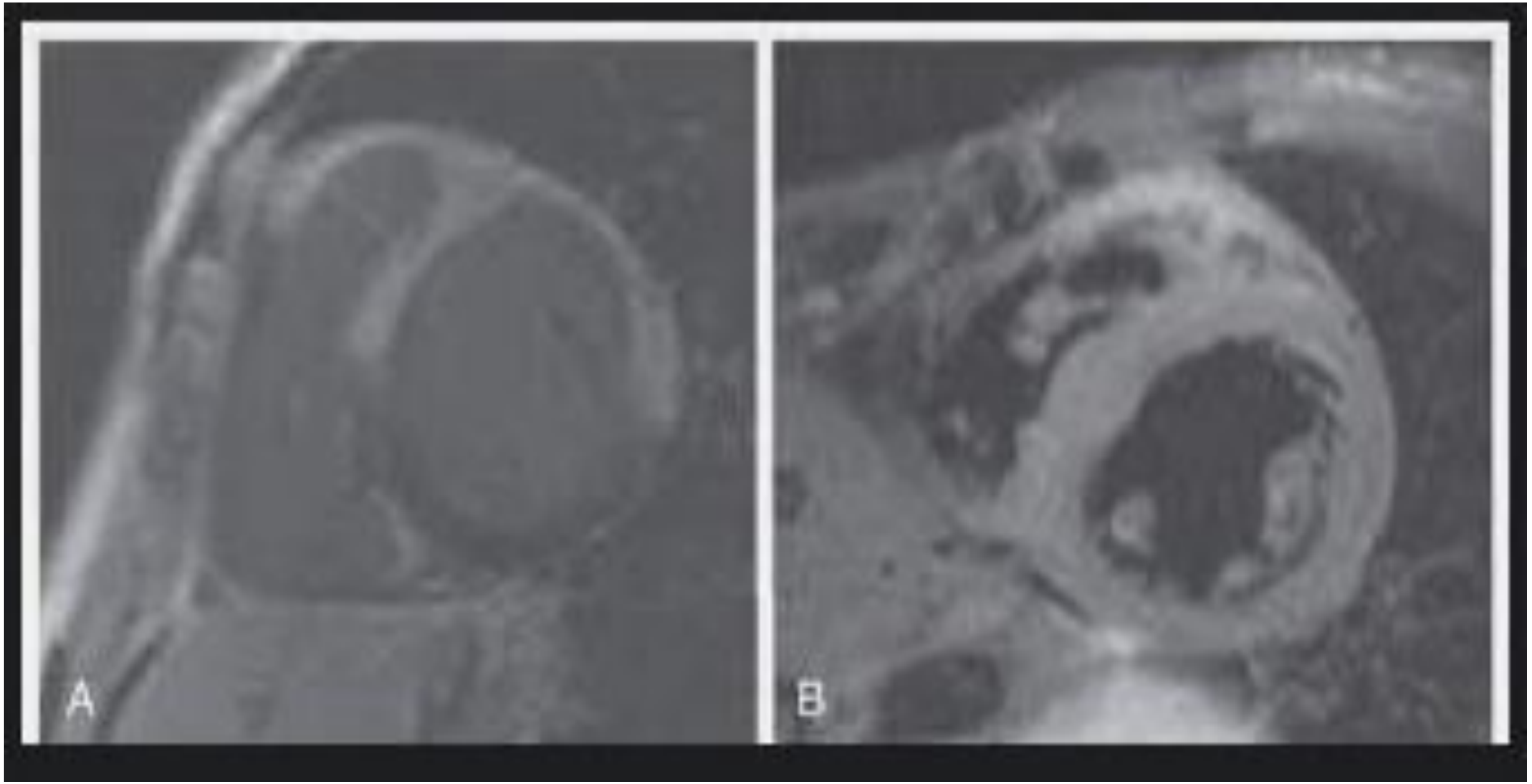
A
B

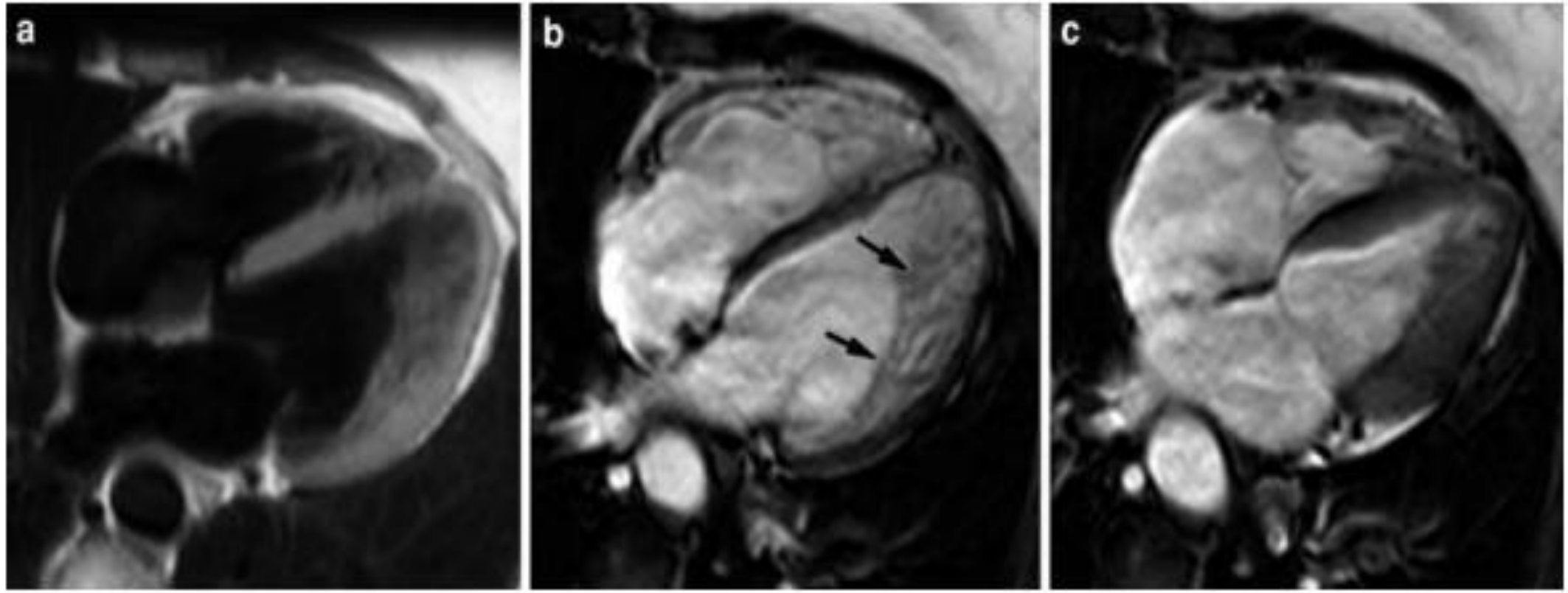

Fig. 3 Dark-blood versus bright-blood imaging in a 56-year-old woman with LV non-compaction cardiomyopathy (LVNC). The patient was referred for MRI because of thickened LV lateral wall on transthoracic echocardiography. T1w-imaging (**a**), cine imaging at end diastole (**b**), and end systole (**c**) in horizontal long-axis. While the LV lateral wall appears thickened on T1w-imaging and end-systolic cine imaging, the prominent trabecular network (*arrows*, **b**) is well visible on end-diastolic cine imaging in the lateral and apical part of the LV, confirming the diagnosis of LVNC. Likely stagnant blood between these prominent trabeculations causes a pseudo-thickening of the lateral wall on dark-blood imaging

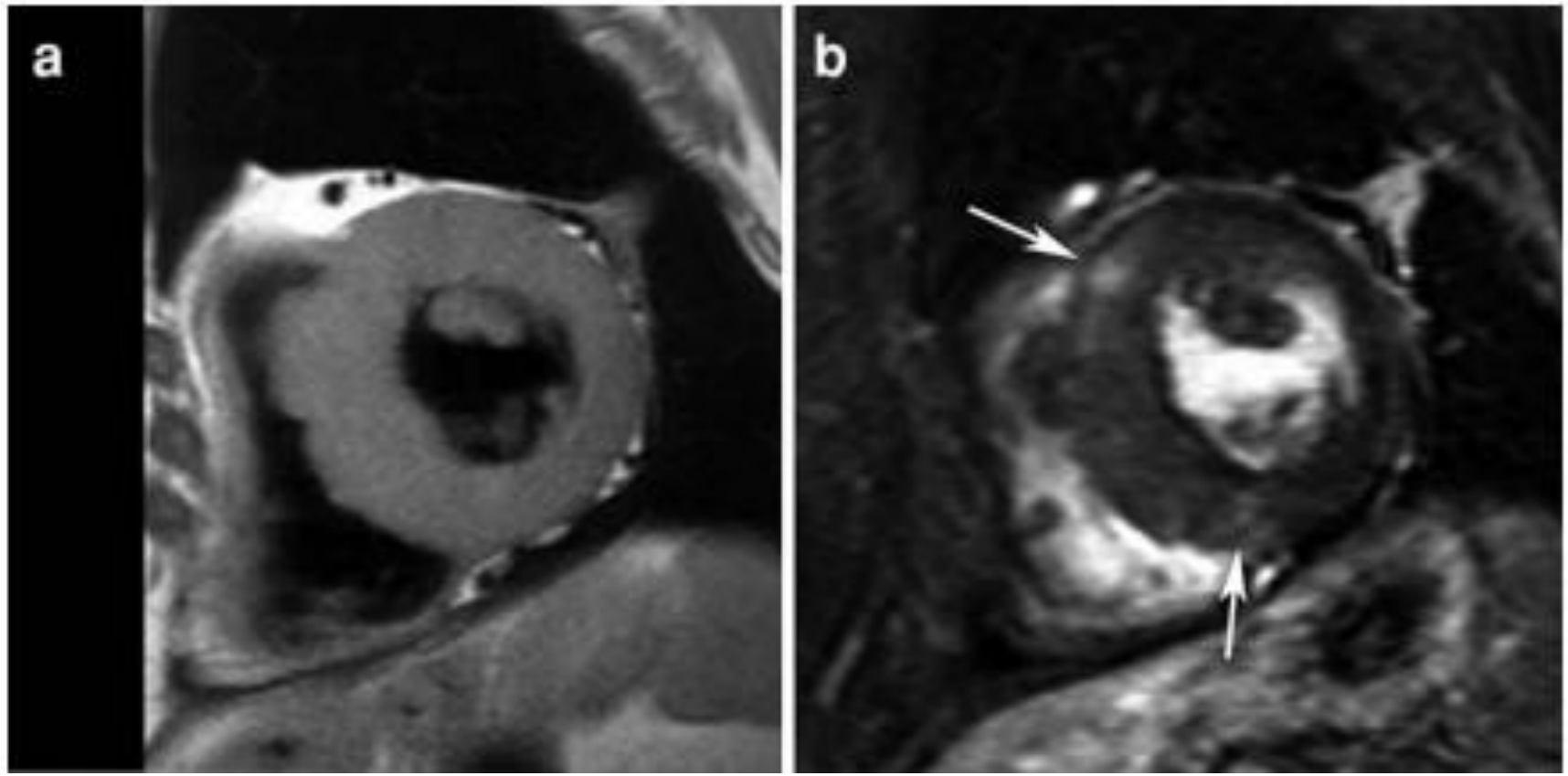

Fig. 8 Comprehensive MRI in a 57-year-old woman with severe form of obstructive hypertrophic cardiomyopathy. T1w-imaging (**a**), late Gd imaging (**b**), cine imaging at end diastole (**c**) and end systole (**d**), and SPAMM myocardial tagging at end diastole (**e**) and end systole (**f**). This approach allows for evaluation of the presence, location and extent of hypertrophy, and for assessment of myocardial wall motion and deformation

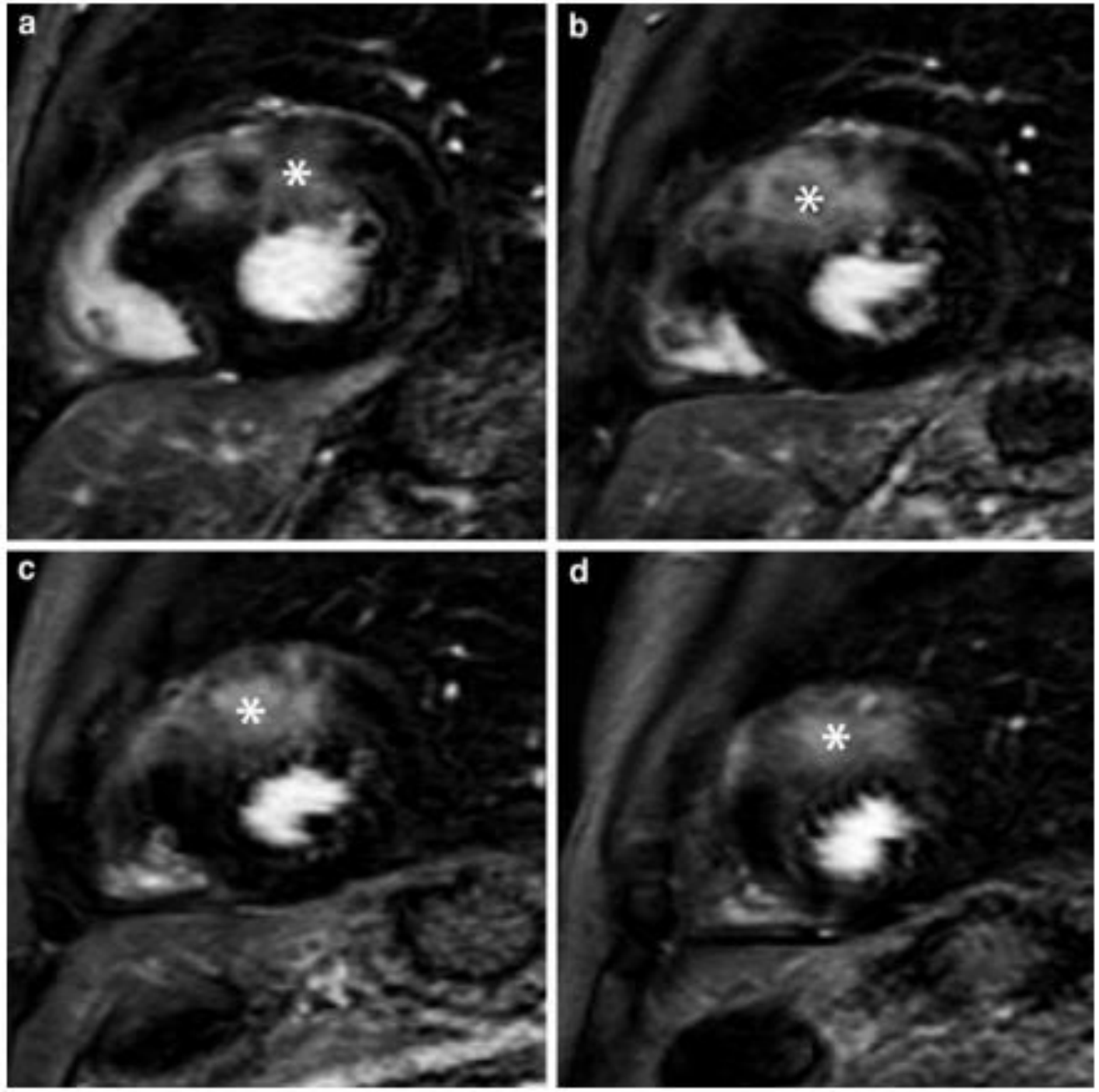
a
b
c
d

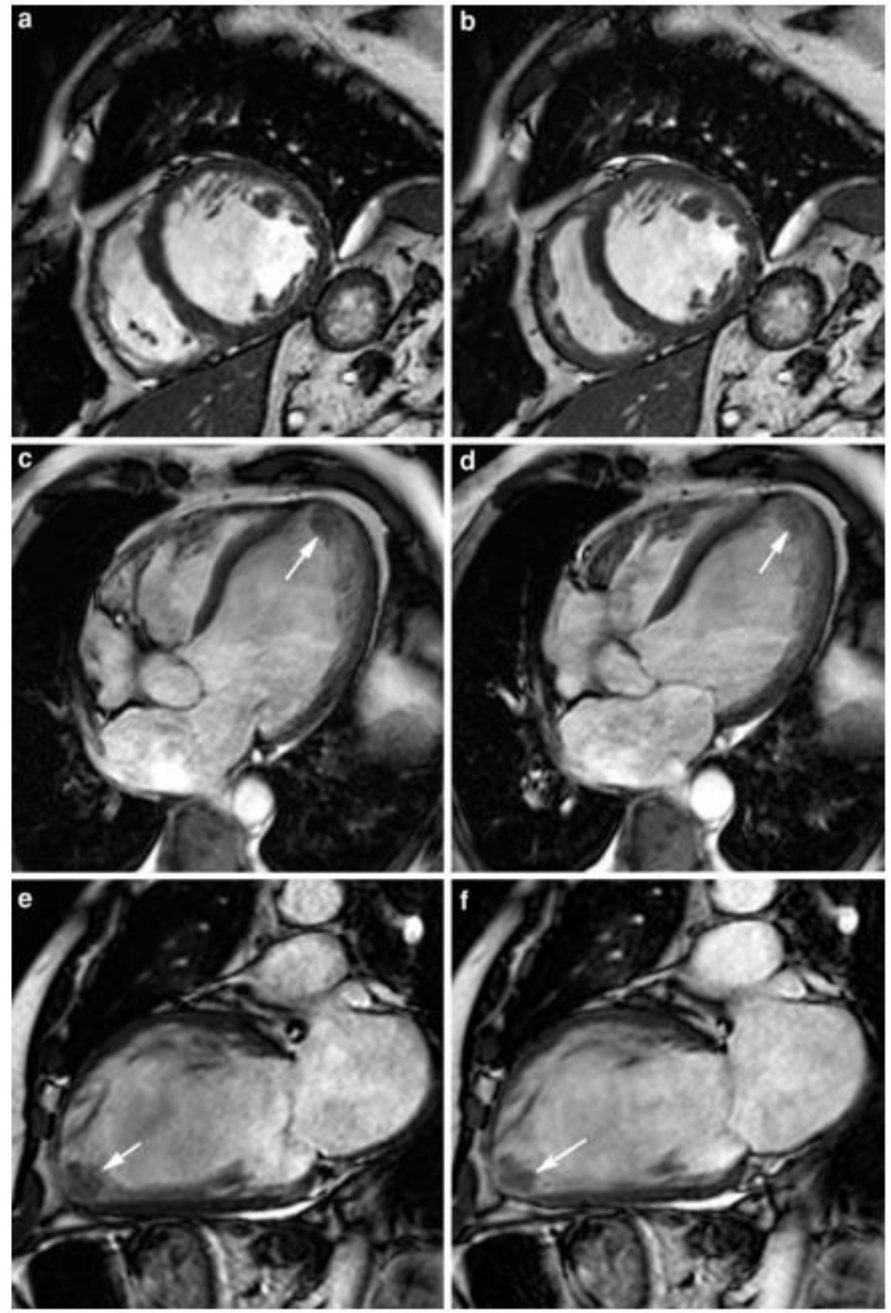

Fig. 23 Idiopathic DCM in a 53-year-old man. Cine imaging in short-axis (**a**, **b**), horizontal long-axis (**c**, **d**), and vertical long-axis (**e**, **f**), at end diastole (*left column*) and end systole (*right column*). Important LV dilation with severely diminished global and regional function (end-diastolic volume: 463 ml, end-systolic volume: 417 ml, stroke volume: 46 ml, ejection fraction: 10%). Mural thrombus in LV apex (*arrow*, **c**–**d**). Note the moderate hypertrophy of the trabeculations along the LV lateral wall, and the left atrial enlargement due to mitral regurgitation secondary to the LV enlargement. No myocardial abnormalities on late Gd imaging (not shown). Normal luminal appearance of coronary arteries on coronary artery catheterization

HCM

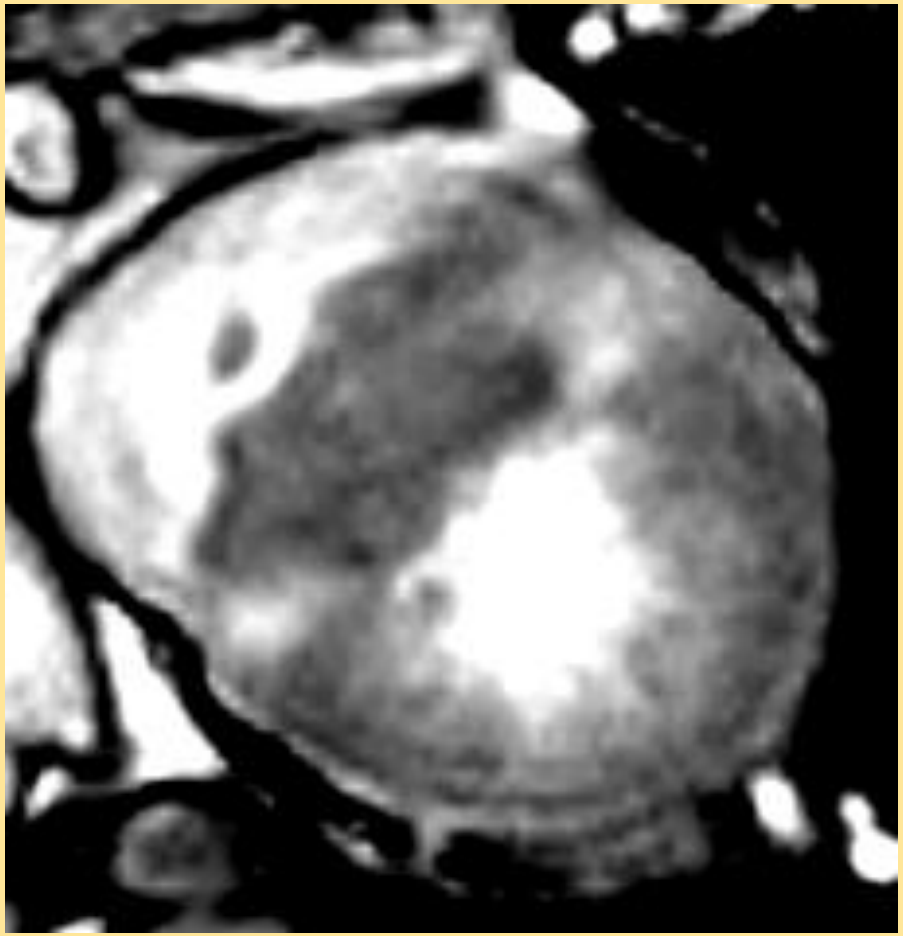

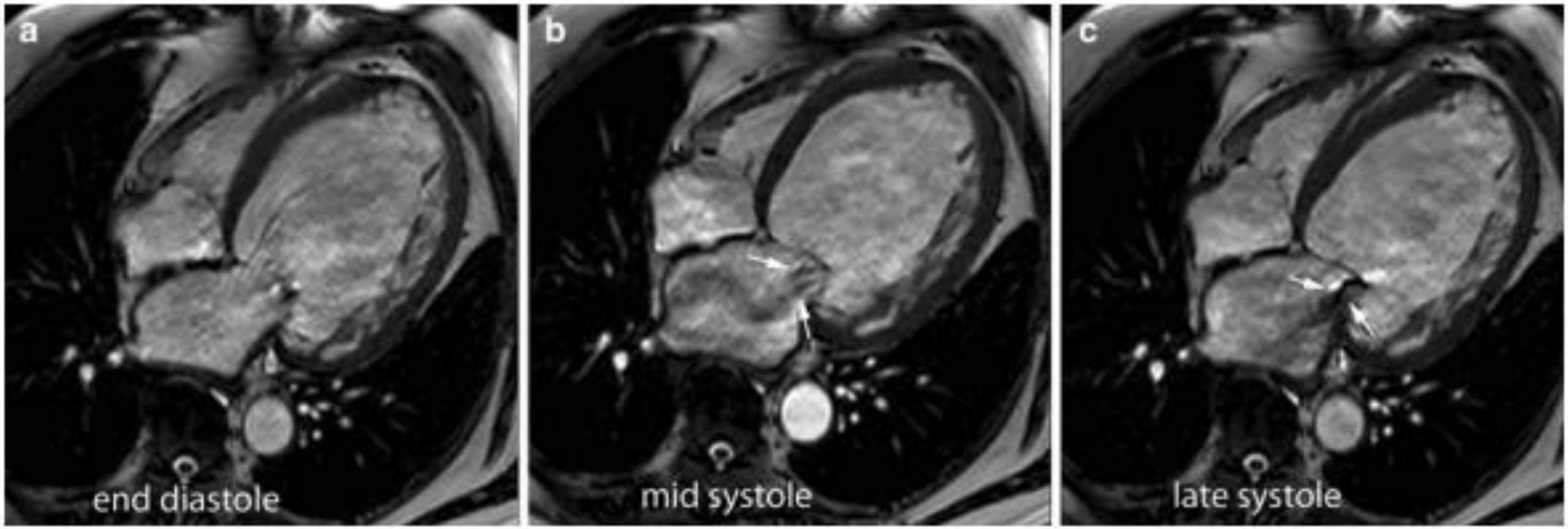

Fig. 24 Extreme form of DCM in a 63-year-old man. Cine imaging in horizontal long-axis at end diastole (**a**), mid systole (**b**), and late systole (**c**). Extreme LV dilatation (EDV: 877 ml, EF: 12%) and moderate RV dilatation (EDV: 248 ml, EF: 42%). Important mitral regurgitation (*arrows*, **b**, **c**) due to mitral valve ring dilatation. Regurgitant volume of 45 ml measured by PC-MRI

Fig. 26 Dilated dysfunctional left ventricle in a 19-year-old woman. Cine imaging in horizontal long-axis (**a**, **b**) and vertical long-axis (**c**, **d**) at end diastole (*left*) and end systole (*right*). Extremely thin-walled ventricles in particular of the ventricular septum, with pronounced appearance of the trabeculations in LV apex (*arrows*, **c**, **d**). The left ventricle has an EDV of 260 ml and EF of 11%. Differentiation between DCM with compensatory trabecular hypertrophy and Left ventricular non-compaction cardiomyopathy (LVNC) is challenging is this case

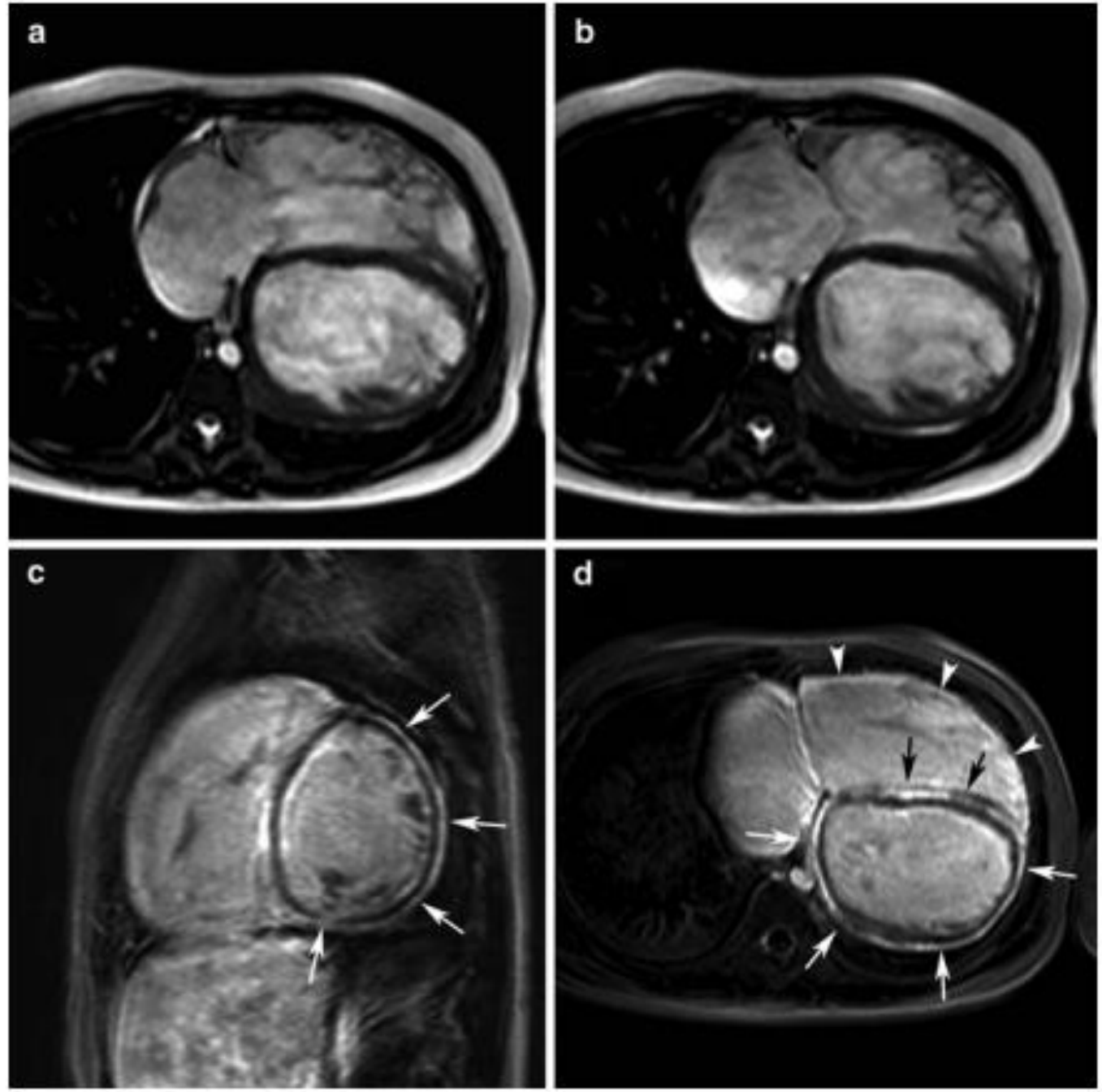

Fig. 27 Extreme form of DCM in an 11-year-old girl involving both ventricles, presenting with heart failure NYHA IV. Cine imaging in horizontal long-axis at end diastole (**a**) and end systole (**b**). Late Gd imaging in short-axis (**c**) and horizontal long-axis (**d**). Important dilatation and dysfunction of both ventricles, i.e., LV EDV: 324 ml, LV EF: 9%, RV EDV: 520 ml, EF: 7%. Late Gd imaging shows diffuse strong enhancement of the subepicardial LV enhancement (*white arrows*, **c**, **d**), midwall septal enhancement (*black arrows*, **d**) and diffuse RV enhancement (*arrowheads*, **d**)

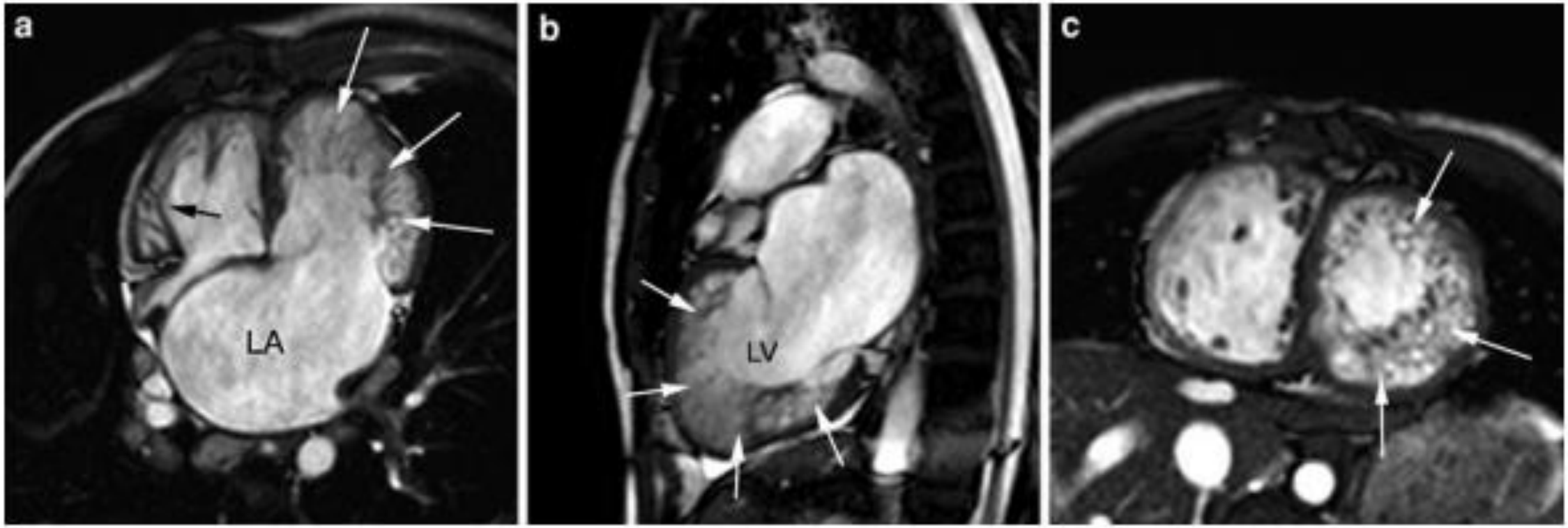

Fig. 38 LVNC in a 26-year-old man. Cine imaging in horizontal long-axis (**a**), vertical long-axis (**b**), and short-axis (**c**). Very prominent trabecular network (*white arrows*) along the entire LV lateral wall and LV apex. Thinning of the compacta of the LV lateral wall. Also in the RV, a prominent network is visible (*black arrow*). Note important dilation of the left atrium (LA)

A trabeculated LV mass value more than 20% predicted the diagnosis of

LVNC

with a sensitivity and specificity of 94 and 94%,respectively.

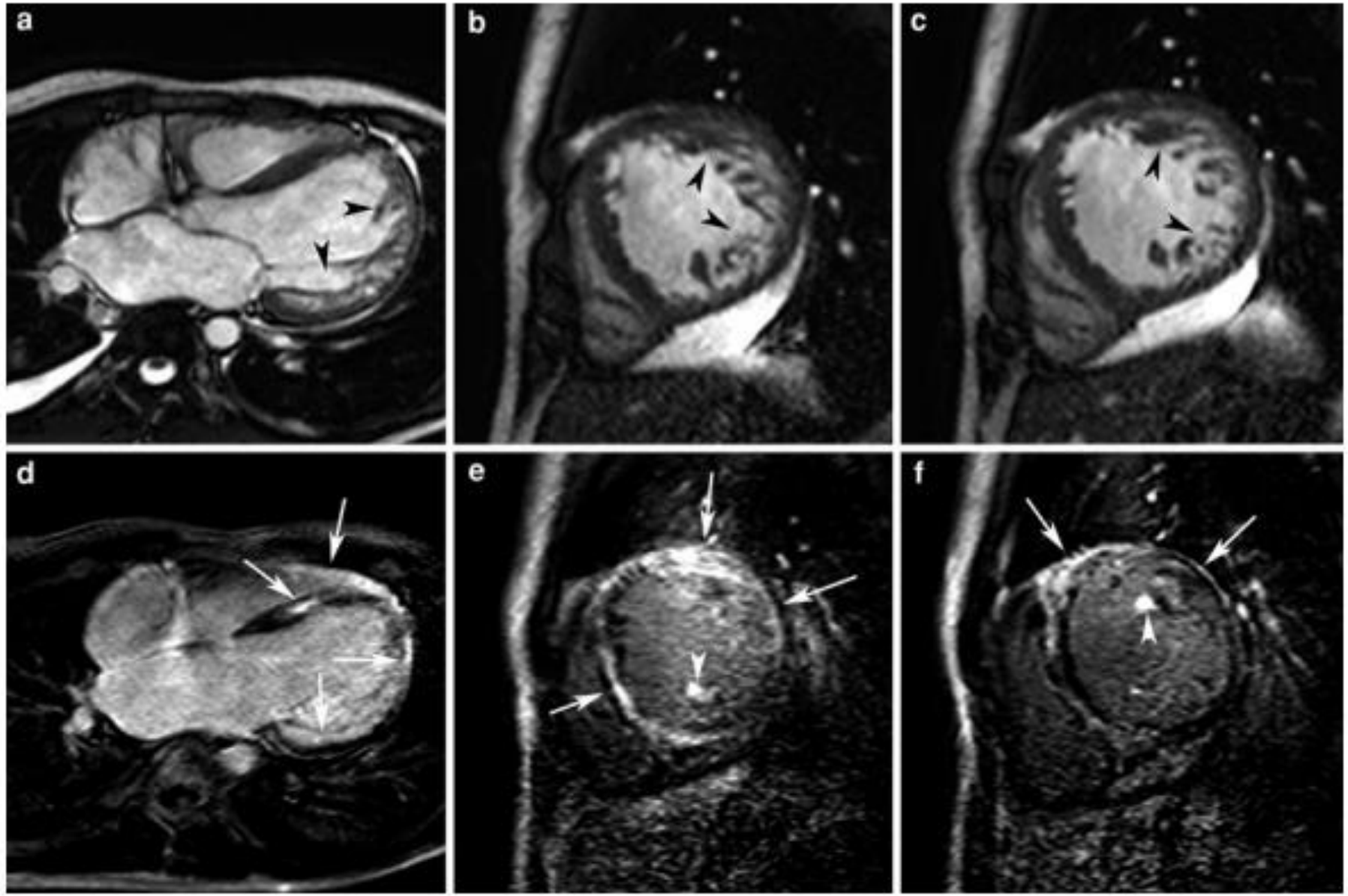

Fig. 40 Myocardial fibrosis in LVNC in a 24-year-old man. Cine imaging in horizontal long-axis (**a**), and short-axis (**b**, **c**). Late Gd imaging in horizontal long-axis (**d**) and short-axis (**e**, **f**). Presence of prominent trabeculations along the LV lateral wall (*arrowheads*, **a**–**c**). Following contrast administration multiple areas of enhancement are seen, in LV anterior wall, midwall of septum, papillary muscles, and RV free wall (*arrows*, **d**–**f**)

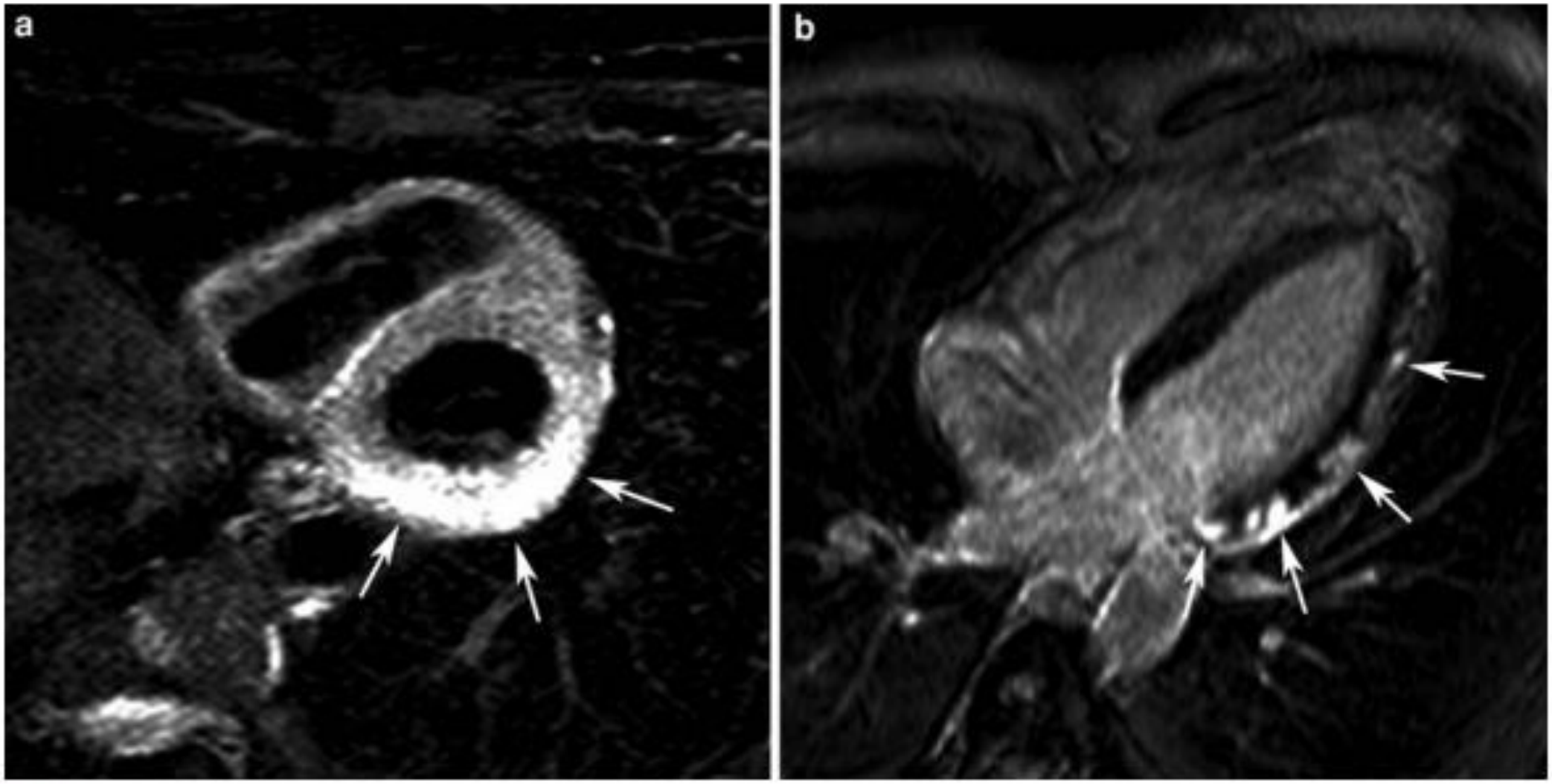

Fig. 42 Acute myocarditis in a 48-year-old man, presenting with acute dyspnea and chest pain, showing increased Troponin I levels (7.4 µg/L), ST-elevations in V4–V6, I, II, aVL, and normal coronary arteries on coronary angiography. Short-axis T2w-imaging (**a**) and horizontal long-axis late Gd imaging (**b**). T2w-imaging shows myocardial edema in infero- lateral wall of the LV (*arrows*, **a**), while late Gd maging shows several subepicardial foci of myocardial enhancement along the lateral wall (*arrows*, **b**) with some associated pericardial enhancement

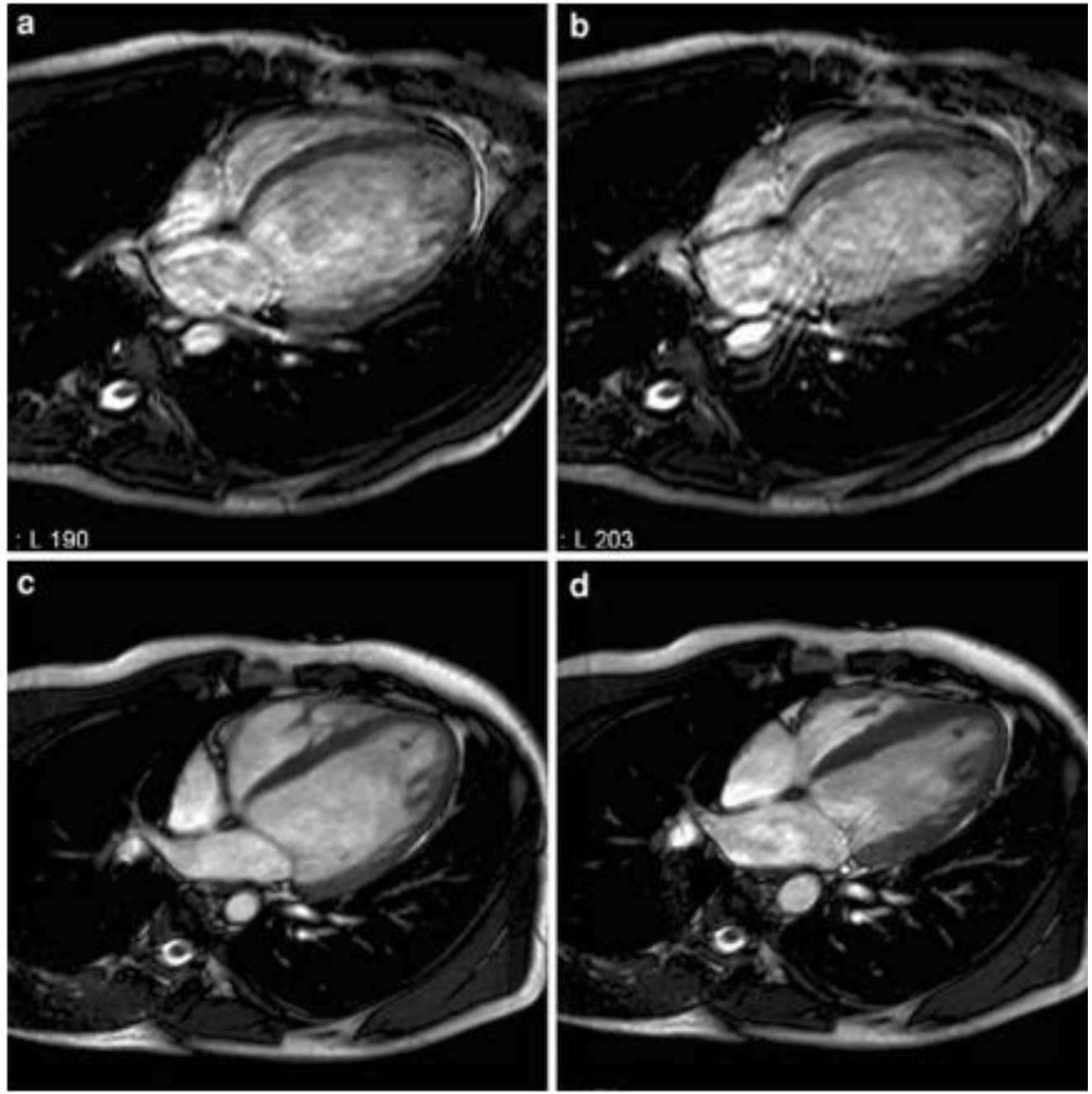

Fig. 49 Tachycardia-induced cardiomyopathy in a 25-year-old man with continuous runs of atrial tachycardia (160/min). Cine imaging before (**a**, **b**), and 9 months following successful ablation (**c**, **d**). End-diastolic (**a**, **c**) and end-systolic (**b**, **d**) time frames. Severe LV dilation (EDV: 504 ml) and systolic dysfunction (EF: 9%) before ablation, with severe motion artifacts due to arrhythmias. Reversed LV remodeling post-ablation with decrease in LV EDV (236 ml) and significant improvement in LV EF (49%)

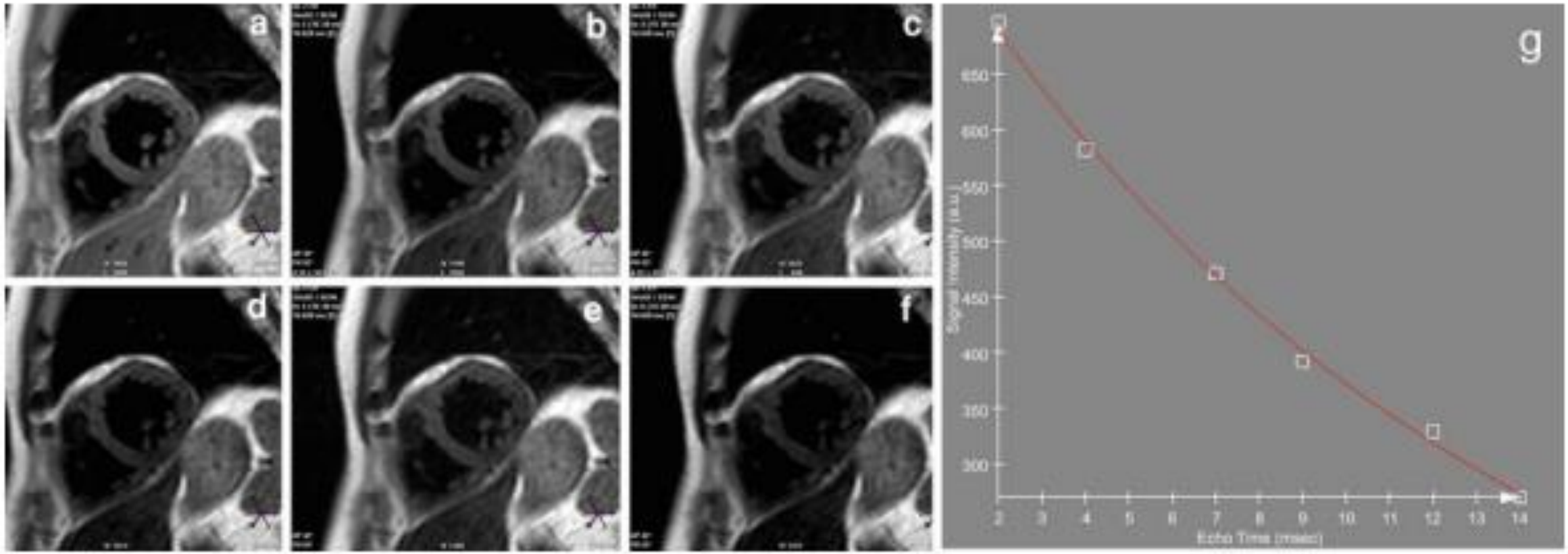

Fig. 53 Hereditary hemochromatosis in a 56-year-old man. T2* imaging using GRASE MRI with 6 echoes (**a**–**f**), and corresponding T2* map (**g**). The myocardial T2* was 13 ms (normal value at 1.5 Tesla: 33.3 ± 7.8 ms). The patient had no evidence of systolic nor diastolic dysfunction

Fig. 58 Cocaine-induced or related myocardial damage (ischemia?, necrosis?, myocarditis?) in a 20-year-old man, who was admitted with ventricular tachycardia and fibrillation. The patient showed ST-segment abnormalities on ECG and elevated cardiac troponins. Late Gd imaging in the vertical long-axis (**a**) and short-axis (**b**) shows well-delineated, focal zone with abnormal transmural enhancement in LV apex (*arrows*)

Fig. 59 Anthracycline cardiotoxicity in a 60-year-old man with previous chemotherapy for osteosarcoma, presenting with cardiac failure. Horizontal long-axis cine imaging at end diastole (**a**) and end systole (**b**), short-axis late Gd imaging (**c**). Important LV dilation and dysfunction (EDV: 269 ml, EF: 23%). Presence of a moderately severe mitral regurgitation. Late Gd imaging shows area of enhancement in LV inferior wall (*arrow*, **c**) (midwall to subepicardium). The enhancement pattern is non-ischemic (the patient presented with normal coronary arteries). Though non-specific, the enhancement is likely to represent myocardial damage (scarring) caused by anthracycline toxicity

RV

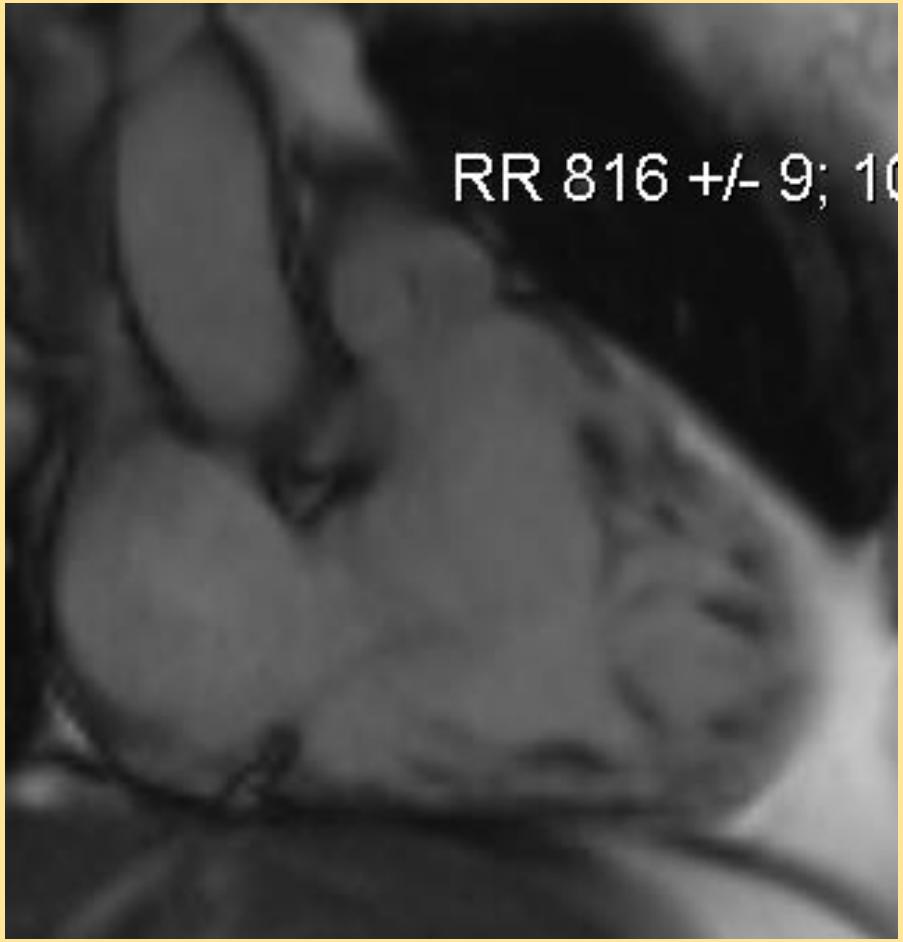

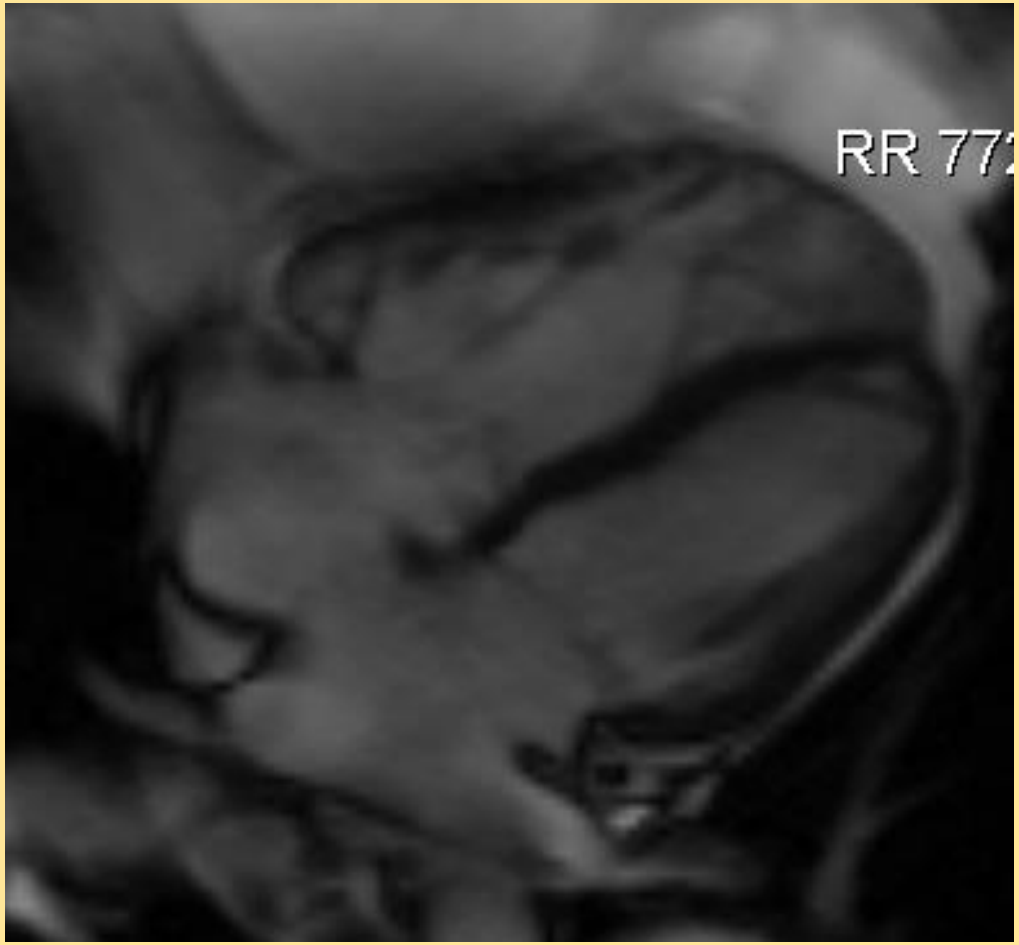

Evaluation of Cardiac Metabolism by Magnetic Resonance Spectroscopy in Heart Failure

Alterations in myocardial energy metabolism as demonstrated by magnetic resonance spectroscopy (MRS) are critically involved in heart failure development. ^{1}H-MRS allows investigation of the role of myocardial lipid accumulation in the pathophysiology of heart failure. With ^{31}P-MRS, the most useful parameter is the cardiac adenosine triphosphate to phosphocreatine ratio, which is typically reduced in the failing heart and correlates with

- T2w-imaging is of interest for depicting myocardial edema in acute myocardial events.
- T2* imaging is the preferred technique to noninvasively measure the presence of myocardial iron deposition and to monitor chelation therapy.
- Contrast-enhanced MRI;LGE, provides accurate information regarding the presence of fibrotic myocardial replacement.
- The pattern/location of enhancement is helpful to discriminate between ischemic and non-ischemic origin.
- T1-mapping techniques yield promising results to depict the presence of diffuse myocardial fibrosis.

Conclusion:

This chapter focuses on the emerging role of MRI to assess heart failure . MRI provides unique information on myocardial tissue characteristics and functional properties, diagnosis, differential diagnosis, follow-up of disease progression, and evaluation of response to treatment of HF.